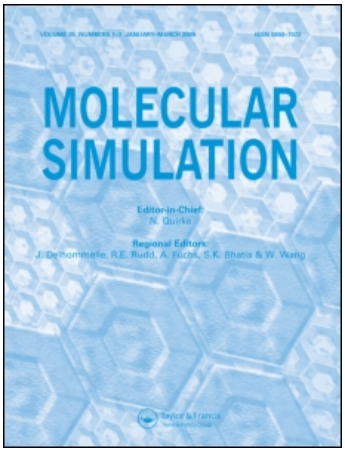

Molecular Simulation
Publication details, including instructions for authors and subscription information:
http://www.informaworld.com/smpp/title~content=t713644482

Surface segregation phenomena in Pt-Pd nanoparticles: dependence on nanocluster size

G. E. Ramirez Caballero[a]; P. B. Balbuena[a]
[a] Department of Chemical Engineering, Texas A&M University, College Station, TX, USA

To cite this Article Caballero, G. E. Ramirez and Balbuena, P. B.(2006) 'Surface segregation phenomena in Pt-Pd nanoparticles: dependence on nanocluster size', Molecular Simulation, 32: 3, 297 — 303
To link to this Article: DOI: 10.1080/08927020600684337
URL: http://dx.doi.org/10.1080/08927020600684337

Molecular Simulation, Vol. 32, Nos. 3–4, 15 March–April 2006, 297–303

Taylor & Francis
Taylor & Francis Group

Surface segregation phenomena in Pt–Pd nanoparticles: dependence on nanocluster size

G. E. RAMIREZ CABALLERO† and P. B. BALBUENA*

Department of Chemical Engineering, Texas A&M University, College Station, TX 77843, USA

(Received December 2005; in final form March 2006)

Classical molecular dynamics (MD) simulations are used to investigate the effect of the nanocluster size on surface segregation phenomena of Pt alloys containing 10, 30, 50, 70 and 90% Pd. Atomic distribution is examined in graphite-supported nanoclusters with approximate diameters of 2 and 4 nm, using a simulated annealing procedure with temperatures varying from 1200 down to 353 K. Following this annealing route, it is found that at concentrations of Pd below a certain threshold, Pt segregates to the surface, whereas Pd segregates to the surface when the overall concentration of Pd is above that threshold. Moreover, the threshold concentration depends on the size, being approximately 50% for the 2 nm nanocluster and in the order of 60% for the 4 nm nanocluster. It is also found that the percent of the surface enriched either in Pt or Pd at a given overall concentration, as well as the nature of the exposed crystallographic faces, depend significantly on the cluster size. Our studies suggest that surface segregation behavior in Pt–Pd supported nanoclusters is influenced by: differences in surface energies, interaction of the clusters with the substrate, and probably most importantly by the fabrication protocol. The implications of these issues on catalytic processes are discussed.

Keywords: Molecular dynamics; Bimetallic particles; Surface segregation; Nanoparticles

1. Introduction

The characterization of surface atomic distribution on bimetallic nanoclusters is of high interest for catalysis, where nanoparticles are used taking advantage of high surface areas and enhanced activities, which in some cases are attributed to particular combination of atoms on the active sites. The need for controlling not only size and shape but also surface composition of alloy nanostructures has been emphasized for specific applications such as the electrocatalytic reactions in fuel cells [1]. In particular, one of the most important questions is how the surface atomic distribution may change as a function of nanocluster size at fixed overall alloy composition.

Surface segregation phenomena has been studied in bulk systems using density functional theory methods [2], and in bimetallic nanoparticles with classical Monte Carlo [3–5] and molecular dynamics (MD) techniques [6,7]. It is clear that atomic surface distribution will depend on the nanoparticle synthesis method; here we explore the variation in surface composition for a particle that has been annealed from temperatures of the order of 1200–353 K. The Pt/Pd system has been selected in our study due to the recently developed interest on these alloys in relation to their significant activity towards the O_2 reduction reaction [8–10], of great importance in low-temperature fuel cells. Several theoretical analyses of Pt–Pd nanoclusters have been recently reported [11–13]. Detailed studies of the effect of composition on the structure of small clusters of less than 100 atoms [11,12] yielded important information about the lowest energy configurations, and their relation to the atomic coordination and number of pure and mixed bonds. An interesting investigation on larger nanoclusters of 456 and 1088 atoms of various compositions provided several insights about melting points and surface energies and

*Corresponding author. Email: balbuena@tamu.edu
†Permanent address: Department of Chemical Engineering, Universidad Industrial de Santander, Bucaramanga, Colombia.

Molecular Simulation
ISSN 0892-7022 print/ISSN 1029-0435 online © 2006 Taylor & Francis
http://www.tandf.co.uk/journals
DOI: 10.1080/08927020600684337

their composition dependence for clusters in vacuum [13]. In this work, we use classical MD simulations to investigate the atomic distribution for Pt–Pd nanoclusters of 2 and 4 nm supported on a graphite slab, at various overall compositions and temperatures.

2. Computational details

Classical MD simulations were performed on bimetallic nanoclusters of Pt–Pd supported on a 2-layers slab of graphite. Two cluster sizes were simulated, one of 2 nm (343 atoms) and another of 4 nm (2194 atoms). For each size several different compositions were investigated: 90%Pt–10%Pd, 70%Pt–30%Pd, 50%Pt–50%Pd, 30%Pt–70%Pd and 10%Pt–90%Pd. To initiate the simulations (at 1200 K), a cubic shape cluster with fcc structure was chosen, with the low composition component located in the center, surrounded by the high composition component. The properties of interest were cluster structure change by surface segregation, atomic mobility towards an equilibrium state, and melting point of the system. One guest atom chemically inert; i.e. non interacting with the metal components of the cluster was located below the cluster and aligned with its center, in such a way that it serves as a reference point to follow cluster structure changes. DL-POLY version 2.14 [14] was used for all the MD simulations.

Annealing simulations of clusters were performed in a range from 1200 to 353.15 K in steps of 100 K. At each temperature, the total simulation time, 1.1 ns, was divided into two periods: the first one, of 1 ns, was estimated to be enough for the cluster to reach an equilibrium state, characterized by a minimum in the total energy and one in which atom segregation to the surface does not occur any more. Except for $T = 1200$ K, the initial configuration for each temperature was taken as that found in the last equilibrated configuration from the previous temperature. Therefore, the effective equilibration time was longer as the temperature was decreasing, for example at 1100 K the system was already run for 1.1 ns at 1200 K, and then equilibrated again for 1 ns, making an effective equilibration time of 2.1 ns; thus at 353 K, the effective equilibration time was close to 11 ns. Since the cluster structure during the initial equilibration period was of no interest, the range of the atomic interactions, given by the cut off radius, was chosen as 10 Å. During the second period of 100 ps, where the statistical properties are computed, the system was already in equilibrium and the final atom distribution became the focus of interest, therefore the cut off was increased and its value was fixed according to the cluster size: 25 and 35 Å for clusters of 2 and 4 nm, respectively.

A histogram was collected saving configurations every 1 ps during the last 100 ps. Statistically averaged radial distribution functions were calculated from this data within spherical shells of 0.05 Å. Fluctuations in the surface atomic distribution vary with temperature. The melting point of the Pt/Pd mixtures is estimated to be in the order of 1200–1500 K [13], and it could be enhanced due to the presence of the substrate, as we shown in previous work [6]. Thus, during the annealing process the mixtures start close to the melting point but gradually become solid-like at temperatures below the melting point. Typical fluctuations δ in the number of surface atoms n of one species calculated over N configurations as:

$$\delta = \frac{1}{N}\left[\sum_{i}^{N}\left(n_i - \langle n\rangle\right)^2\right]^{1/2}$$

are in the order of 0.05 (for a total of 150 surface atoms in the 2 nm cluster) at 353 K.

With the radial distribution $g_{ab}(r)$ and the $n_{ab}(r)$ function, that is the average number of atoms of type "b" within a sphere of radius r around an atom of type "a", is possible to calculate the number of atoms at a certain distance from the guest atom and, taking advantage of the quasi-spherical final shape of the cluster, calculate the number of atoms on the surface, statistically averaged over many equilibrated configurations. At high temperatures, the cluster has certain mobility over the surface, which may cause the reference atom to become misaligned. For this reason, the position of the reference atom was always reset immediately before the production period (figure 1).

The MD simulations were carried out in a canonical ensemble [15] at constant temperature using the Berendsen thermostat [16] with a temperature relaxation time of 0.4 ps; the number of particles and the volume were kept constant; the simulations were carry out without periodic boundary conditions. The simulation box has dimensions $x = 108$ Å, $y = 144.24$ Å and $z = 108$ Å.

The semi-empirical many-body Sutton–Chen potential [17] was chosen to govern the behavior of Pt–Pt, Pt–Pd, and Pd–Pd interactions. This potential model includes the effect of the local electron density to account for the many-body terms.

The Sutton–Chen potential energy can be expressed as [17]:

$$U_{\text{tot}} = \varepsilon_{\text{SC}}\left[\frac{1}{2}\sum_{i\neq j}\sum\left(\frac{a}{r_{ij}}\right)^n - c\sum_i \rho_i^{1/2}\right] \qquad (1)$$

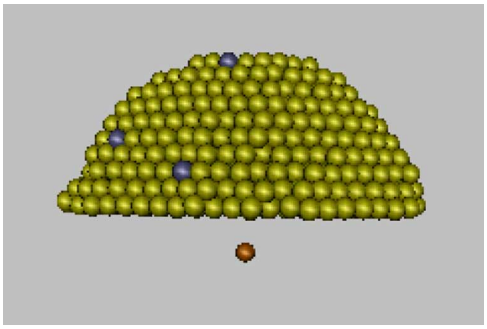

Figure 1. Snapshot of a bimetallic cluster of 4 nm in its equilibrated configuration at $T = 400$ K, with overall composition 90%Pt/10%Pd, showing the location of an inert reference atom used to calculate the atomic distribution in the cluster. The cluster is supported by a graphite substrate (not shown).

Table I. Parameters of the Sutton–Chen potential. For Pt–Pd interactions the parameters were calculated with the following expressions: $m^{AB} = (1/2)(m^{AA} + m^{BB})$, $n^{AB} = (1/2)(n^{AA} + n^{BB})$, $a^{AB} = (a^{AA}a^{BB})^{1/2}$, $\varepsilon_{SC}^{AB} = (\varepsilon_{SC}^{AA}\varepsilon_{SC}^{BB})^{1/2}$.

	a (Å)	ε_{SC} (10^{-2} eV)	m	n	c
Pt–Pt	3.92	1.9835	8	10	34.428
Pt–Pd	3.90	0.9104	7.5	11	
Pd–Pd	3.89	0.4179	7	12	108.526

Table II. LJ parameters of Pt–C [19] and Pd–C [20] interactions obtained using the Lorentz–Berthelot mixing rules.

	ε (10^{-2} eV)	σ (Å)
Pt–C	4.0922	2.936
Pd–C	3.2700	2.990

where

$$\rho_i = \sum_{j \neq i} \left(\frac{a}{r_{ij}} \right)^m \tag{2}$$

The first term of the equation (1) describes the pair-wise repulsive potential and the second term describes the metallic bonding energy associated with ρ_i which represents the local electron density.

For the description of Pt–Pt, Pt–Pd, Pd–Pd interactions, the following parameters were adopted [18] (table I).

For the description of Pd–C and Pt–C interactions, the 6–12 Lennard–Jones (LJ) potential [15] was adopted, with length σ and energy ε parameters (table II).

The Sutton–Chen potential has proved useful in optimizations of transition metal cluster structures and search of their global minimum [21], and to describe static and dynamic properties of transition and noble metals, such as bulk moduli and elastic constants [17], as well as surface energies, stress tensor components and surface relaxation of fcc metals [22]. A similar potential function has been developed for binary fcc metallic alloys and it was applied for calculating the concentration dependencies of the lattice parameters, elastic constants and enthalpy of mixing of fcc binary alloys [18]. Several applications to pure metal and alloy nanoclusters using this potential [23,24] and its most recent modification, the quantum-Sutton–Chen potential [25] has been applied to the same system, Pt–Pd nanoclusters [13].

3. Results and discussion

3.1 Description of the system once equilibrium is reached

Once equilibrium has been reached at a given temperature, for both sizes, the supported cluster adopts an approximately hemispherical shape with different types of crystal structure on its external walls. On the surface of the clusters, for both sizes, Pt atoms tend to agglomerate with others of the same species forming small islands, whereas Pd atoms tend to form chains, which, in some cases, seem to enclose domains of Pt, as shown in figures 2 and 3. The side view of figure 2 (right image) depicts five layers of atoms of the 50–50% 2 nm cluster that conform the cluster structure in the direction perpendicular to the substrate,

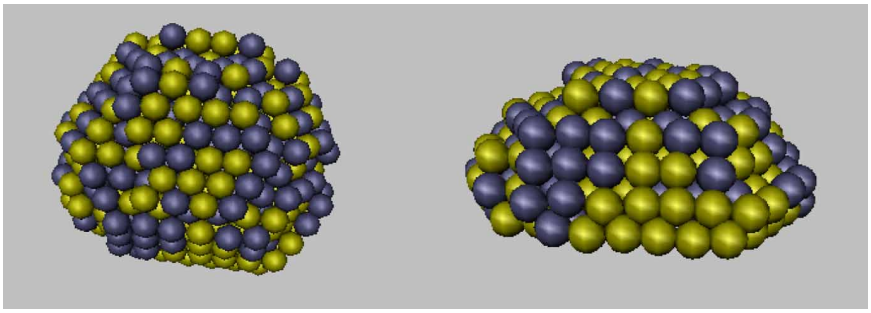

Figure 2. Cluster of 2 nm 50%Pt–50%Pd. Left, top view; Right, side view. The blue atoms are Pd and the gold atoms are Pt.

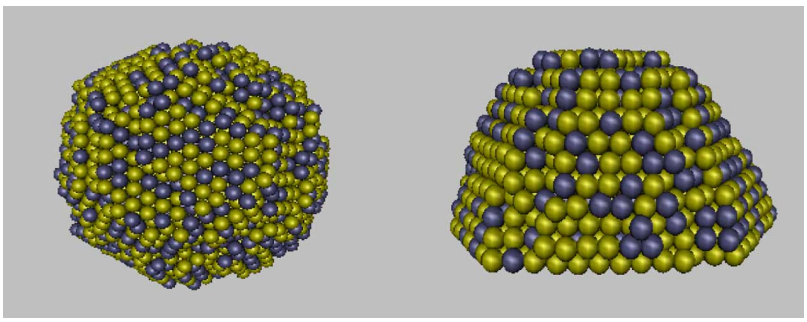

Figure 3. Cluster of 4 nm 50%Pt/50%Pd. Note the formation of chains by the Pd atoms (blue) and the more extended islands formed by the Pt atoms (colored gold).

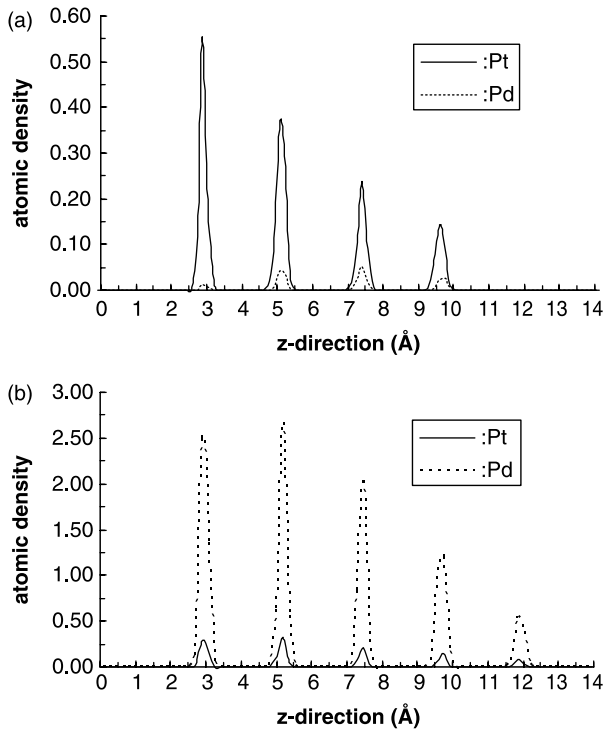

Figure 4. Atomic density of Pt and Pd at 353 K in a direction z perpendicular to the substrate, located at $z = 0$. (a) 90%Pt–10%Pd; (b) 10%Pt–90%Pd.

with the base wetting layer being that with the largest area. Interestingly, all of the 2 nm clusters are made up of five layers, except for the 90%Pt–10%Pd in which the number of layers is only four, as illustrated by the density profile in the direction perpendicular to the substrate shown in figure 4. The cluster morphology at a given composition is determined both by metal–metal and metal–carbon interactions, and in the case of Pt-rich clusters it seems that the metal–carbon interactions dominate determining a decrease in the total number of layers in the direction perpendicular to the substrate. Figure 3 shows the top and side views for a 4 nm cluster and 50%Pt–50%Pd overall composition. Eleven layers of atoms conform the cluster. Similarly to the behavior in the 2 nm cluster, all of the 4 nm clusters are made up of eleven layers except for the 90%Pt–10%Pd in which the number of layers is only 10.

The most typical crystallographic faces found on the clusters were (1,1,1) and (1,0,0), however, crystal structures of (1,1,0) were also found, though in lower proportion. These faces are illustrated in figure 5. We have also examined the average surface bond lengths as a function of composition and cluster size. The average Pd–Pd and Pt–Pd surface bond lengths were found 2.73 Å, for all compositions, whereas the Pt–Pt surface bond length was also 2.73 Å for all compositions in the 4 nm cluster, but shorter average values, of 2.67 Å were found at compositions between 30 and 70% Pt, where the Pt atoms form small islands on the surface (figure 2).

3.2 *Surface segregation*

The equilibrium distribution of metal atoms on the surface of the cluster, for each size, overall composition and temperature, were obtained from the radial distribution of components around the guest atom, as explained in the methodology section. Those compositions can be expressed as Pd percentage as shown in tables 3 and 4.

Data shows a trend in the Pd composition on the cluster surface with respect to the total Pd content in the cluster: At low overall Pd composition (10 and 30%) the average percentage of this metal on the cluster surface is lower than the total, whereas at high total composition (70 and 90%) the average percentage on the surface is higher than the total. This trend is observed for both cluster sizes. These data may be interpreted in terms of surface segregation: the metal with higher composition in the cluster is more segregated towards the surface independently of the cluster size and overall composition.

For the 50% total Pd in the cluster, the average percentage on the surface equals the overall composition for the 2 nm cluster, whereas continues to be lower than the total composition for the 4 nm cluster. Figure 6 suggests an interesting exception to the described trend: for the case of compositions between 50 and 60% Pd in the cluster of 4 nm, Pt is more segregated even though its overall composition is lower than that of Pd. Thus, another trend is observed, (tables 3 and 4; figure 6), in terms of segregation depending upon cluster size: at each overall composition, the higher composition component is more segregated in 4 nm than in 2 nm clusters.

Surface energies for bulk metals have been reported by Ruban *et al.* [2], 1.03 eV/atom for Pt and 0.84 eV/atom for Pd, and according to their study there should be no segregation for systems where Pd is an impurity of a Pt host, and moderate antisegregation of the solute Pt in Pd matrices. Segregation of Pd in Pd-rich systems, i.e. antisegregation of Pt, is observed in our simulations, and

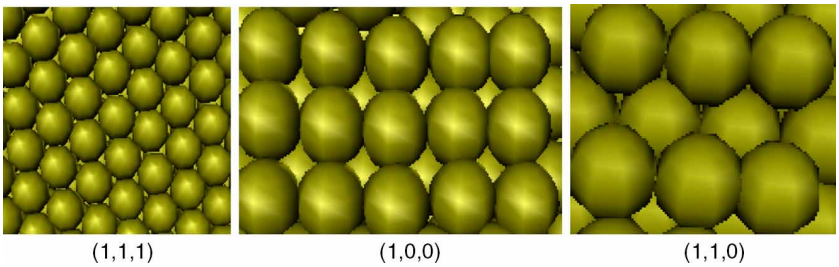

Figure 5. Various types of crystallographic faces detected on the cluster surfaces.

Table III. Percentage of Pd with respect to the total number of atoms on the surface of 2 nm clusters at various temperatures and compositions.

	2 nm cluster				
T (K)	*90%Pt–10%Pd*	*70%Pt–30%Pd*	*50%Pt–50%Pd*	*30%Pt–70%Pd*	*10%Pt–90%Pd*
1000	7.19	30.92	55.40	79.57	93.24
900	8.89	27.17	51.88	78.26	92.55
800	5.07	28.57	53.68	71.59	92.17
700	6.40	30.76	51.28	68.83	92.76
600	6.56	30.83	46.55	78.33	92.00
500	6.40	27.72	48.24	73.39	89.77
400	6.35	25.00	48.10	75.49	88.31
353.15	6.40	28.77	50.52	80.51	91.60
Average	6.65	28.72	50.71	75.75	91.55

Table IV. Percentage of Pd with respect to the total number of atoms on the surface of 4 nm clusters at various temperatures and compositions.

	4 nm cluster				
T (K)	*90%Pt–10%Pd*	*70%Pt–30%Pd*	*50%Pt–50%Pd*	*30%Pt–70%Pd*	*10%Pt–90%Pd*
1000	3.68	20.41	36.22	80.71	95.55
900	3.70	20.05	35.78	80.20	96.04
800	3.52	19.69	35.57	80.41	96.18
700	3.62	19.96	35.36	80.30	96.15
600	3.62	20.04	35.54	79.96	96.19
500	3.94	19.96	35.15	79.84	96.39
400	3.83	19.88	35.48	80.17	96.25
353.15	3.64	19.84	35.49	80.17	96.27
Average	3.71	19.98	35.69	80.23	96.10

no segregation of Pd in the Pt-rich systems. Although our results agree with the general trends suggested by Ruban *et al.* other researchers have found preferential segregation of Pd over Pt [11–13]. There is an important difference in our systems with respect to those reporting preferential Pd segregation, which is the interaction of the clusters with the substrate, that contributes modifying the surface segregation behavior.

3.3 Compositions inside the cluster

In order to study the metal composition inside the cluster, four shells were traced at different radius, taking the guest atom as the center of each shell region. Figure 7 shows the Pd percentage at each surface layer for the 2 nm cluster at 353.15 K. Considering layers 1, 3, and 4, it is apparent that at low Pd composition, 10 and 30%, the Pd content decreases from the core to the surface, whereas at high Pd composition, 70 and 90%, the Pd content increases from the interior to the surface. These observations are in agreement with the trend already described: the higher content component segregates towards the cluster surface. Layer 2, the second inner layer, shows deviations to this rule, reaching a maximum or a minimum value depending on the overall concentration. The 50% Pd cluster shows strong oscillations in the atomic distribution, and does not follow the general trend.

Similar layer-by-layer atomic distribution is shown in figure 8 for clusters of 4 nm and different compositions at 353.15 K, confirming the general trend: the higher content component segregates toward the surface. The atomic distribution in the larger cluster shows much more smooth behavior than that for the 2 nm cluster, with no extreme points. Also, segregation augments as the cluster size increases from 2 to 4 nm as it was already observed from tables 3 and 4. On the other hand, again, the 50% Pd cluster shows the higher composition oscillations and does not conform to the general trend.

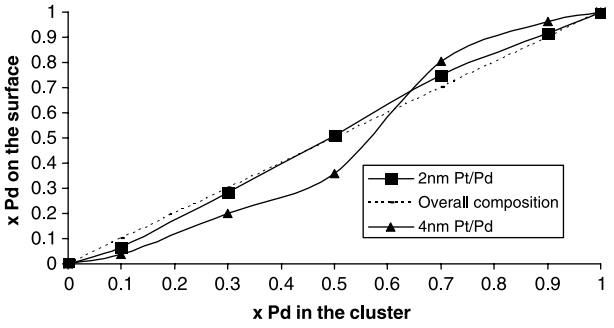

Figure 6. Composition of Pd on the surface as a function of overall Pd composition in the 2 and 4 nm clusters. The dotted line corresponds to the overall composition, shown as a reference.

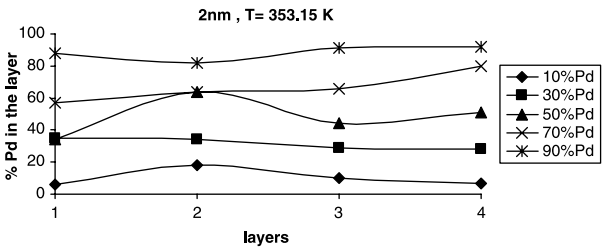

Figure 7. Layer by layer composition for various overall compositions of Pd in a 2 nm particle at 353.15 K. Layer 4 is the outside cluster surface.

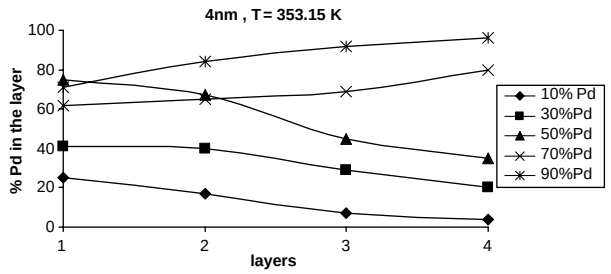

Figure 8. Layer by layer composition for various overall compositions of Pd in a 4 nm particle at 353.15 K. Layer 4 is the outside cluster surface.

The difference of surface energies between Pt and Pd is minimal, as it is their size difference, and this causes other thermodynamic forces to play a role. In particular, in the presence of the surface which interacts more strongly with Pt affecting the surface distribution, especially in Pt-rich nanoclusters where Pt (instead of Pd) is found on the surface in higher proportion than its overall composition. To further investigate the stability of the structures found in these simulations, we calculated equilibrated structures where the opposite segregation behavior is obtained. For example, we did extensive comparisons for overall compositions of 10, 30 and 50 Pd, where the initial configurations were biased to Pd segregated systems. Indeed, local minima are also found for Pd segregated systems at 10, 30 and 50 Pd overall compositions; however, their total energies differed only in 0.01 eV/atom (for clusters of 2 nm) and 0.001 eV/atom (in 4 nm clusters). Therefore, surface segregation behavior in Pt–Pd supported nanoclusters is influenced by: differences in surface energies, interaction of the clusters with the substrate, and probably most importantly by the fabrication protocol.

These conclusions are very relevant for catalytic processes, for example the Pt/Pd combination has been proposed as a good alternative catalyst for the oxygen reduction reaction and the reported analysis of the experimental results is based on the assumption that there is a monolayer of Pt over a Pd nanoparticle [8]. These molecular simulation results illustrate that thermodynamically stable Pt surface monolayers could be obtained at compositions of ~70% Pt, as shown in figure 9, yielding surface compositions of ~71% Pt for a 2 nm particle and ~80% Pt for a 4 nm particle. Further, the Pd atoms are more disconnected from each other in the 4 nm than in the 2 nm cluster, where they form small islands. We emphasize that energetically equivalent systems having an opposite segregation behavior could result from a different synthesis process. In addition, the present simulations do not include the electrochemical environment, neither the adsorption of reactants and intermediate species that may dramatically change not only shape but also atomic distribution.

4. Conclusions

Surface segregation behavior in Pt–Pd supported nanoclusters is influenced by: differences in surface energies, interaction of the clusters with the substrate, and probably most importantly by the fabrication protocol. In this work, the surface atomic distribution of Pt–Pd nanoclusters of 2 and 4 nm diameters has been analyzed using classical MD simulations. The equilibration time at each temperature was of 1 ns, and the systems were annealed from 1200 to 353 K, in intervals of 100 K. Such equilibration times are estimated long enough to account for the different equilibration kinetics of the two nanoclusters. It is found that the surface is enriched in the component present in highest proportion, but the percent of the enhancement is higher for the larger cluster. The layer-by-layer distribution in the 4 nm cluster shows a monotonic increasing trend from the core to the surface for the segregating element; but such trend is less smooth for the 2 nm cluster, where some oscillations are found in the composition profile.

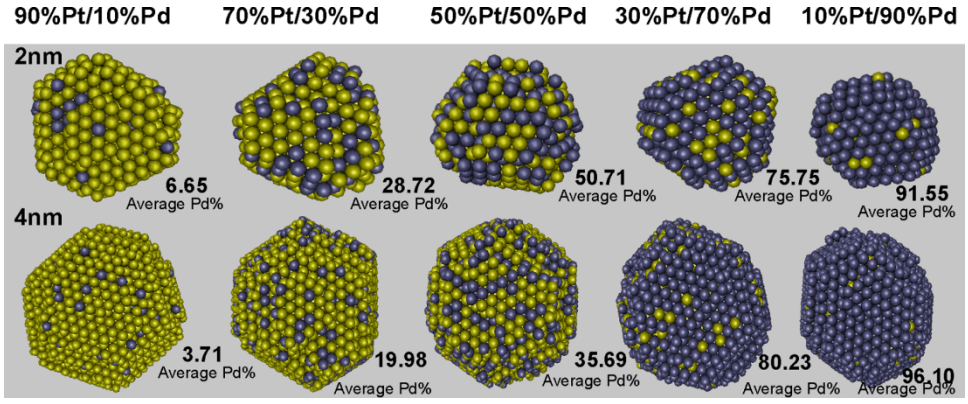

Figure 9. Comparison of surface atomic distribution for the 2 and 4 nm clusters at various compositions of Pt (gold color) and Pd (blue color) at 353.15 K.

Acknowledgements

This work was supported by the Department of Energy, grant DE-FG02-05ER15729. This research used resources of the National Energy Research Scientific Computing Center, which is supported by the Office of Science of the US Department of Energy under Contract No. DE-AC03-76SF00098. We thank Sergio R. Calvo for numerous discussions.

References

[1] H.A. Gasteiger, S.S. Kocha, B. Sompalli, F.T. Wagner. Activity benchmarks and requirements for Pt, Pt-alloy, and non-Pt oxygen reduction catalysts for PEMFCs. *Appl. Catal. B: Environ.*, **56**, 9 (2005).

[2] A.V. Ruban, H.L. Skriver, J.K. Norskov. Surface segregation energies in transition-metal alloys. *Phys. Rev. B*, **59**, 15990 (1999).

[3] D.S. Mainardi, P.B. Balbuena. MonteCarlo Simulation studies of surface segregation in copper–nickel nanoclusters. *Langmuir*, **17**, 2047 (2001).

[4] D.S. Mainardi, P.B. Balbuena. Surface segregation in bimetallic nanoclusters: geometric and thermodynamic effects. *Int. J. Quantum Chem.*, **85**, 580 (2001).

[5] G. Wang, M.A. VanHove, P.N. Ross, M.I. Baskes. Monte Carlo simulations of segregation in Pt–Ni catalyst nanoparticles. *J. Chem. Phys.*, **122**, 024706 (2005).

[6] S.-P. Huang, P.B. Balbuena. Melting of bimetallic Cu–Ni nanoclusters. *J. Phys. Chem. B*, **106**, 7225 (2002).

[7] F. Baletto, C. Mottet, R. Ferrando. Growth simulations of silver shells on copper and palladium nanoclusters. *Phys. Rev. B*, **66**, 155420 (2002).

[8] J. Zhang, Y. Mo, M.B. Vukmirovic, R. Klie, K. Sasaki, R.R. Adzic. Platinum monolayer electrocatalysts for O-2 reduction: Pt monolayer on Pd(111) and on carbon-supported Pd nanoparticles. *J. Phys. Chem. B*, **108**, 10955 (2004).

[9] J. Zhang, M.B. Vukmirovic, Y. Xu, M. Mavrikakis, R.R. Adzic. Controlling the catalytic activity of platinum-monolayer electrocatalysts for oxygen reduction with different substrates. *Angew. Chem. Int. Ed.*, **44**, 2132 (2005).

[10] Y. Wang, P.B. Balbuena. Design of oxygen reduction bimetallic catalysts: *ab-initio* derived thermodynamic guidelines. *J. Phys. Chem. B*, **109**, 18902 (2005).

[11] G. Rossi, R. Ferrando, A. Rapallo, A. Fortunelli, B.C. Curley, L.D. Lloyd, R.L. Johnston. Global optimization of bimetallic cluster structures. II. Size-mismatched Ag–Pd, Ag–Au, and Pd–Pt systems. *J. Chem. Phys.*, **122**, 194309 (2005).

[12] L.D. Lloyd, R.L. Johnston, S. Salhi, N.T. Wilson. Theoretical investigation of isomer stability in platinum-palladium nanoalloy clusters. *J. Mater. Chem.*, **14**, 1691 (2004).

[13] S.K.R.S. Sankaranarayanan, V.R. Bhethanabotla, B. Joseph. Molecular dynamics simulations of the melting of Pt–Pd nanoclusters. *Phys. Rev. B*, **71**, 195415 (2005).

[14] W. Smith, T.R. Forester. *DL_POLY*, Daresbury Laboratory, Daresbury (1996).

[15] M.P. Allen, D.J. Tildesley. *Computer Simulation of Liquids*, Oxford University Press, Oxford (1990).

[16] H.J.C. Berendsen, J.P.M. Postma, W.F.V. Gunsteren, A.D. Nola, J.R. Haak. Molecular dynamics with coupling to an external bath. *J. Chem. Phys.*, **81**, 3684 (1984).

[17] A.P. Sutton, J. Chen. Long-range Finnis-Sinclair potentials. *Philos. Mag. Lett.*, **61**, 139 (1990).

[18] H. Rafii-Tabar, A.P. Sutton. Long-range Finnis–Sinclair potentials for f.c.c. metallic alloys. *Philos. Mag. Lett.*, **63**, 217 (1991).

[19] S.R. Calvo, P.B. Balbuena. Molecular dynamics studies of phonon spectra in mono- and bimetallic nanoclusters. *Surf. Sci.*, **581**, 213 (2005).

[20] P. Brault, A.L. Thomann, C. Andreazza-Vignolle, P. Andreazza. Tuning growth from clusters to continuous ultrathin films: experiments and molecular dynamics simulations of Pd plasma sputter deposition. *Eur. Phys. J.-Appl. Phys.*, **19**, 83 (2002).

[21] J.P.K. Doye, D.J. Wales. Global minima for transition metal clusters described by Sutton–Chen potentials. *New J. Chem.*, 733 (1998).

[22] B.D. Todd, R.M. Lynden-Bell. Surface and bulk properties of metals modelled with Sutton–Chen potentials. *Surf Sci.*, **281**, 191 (1993).

[23] H. Rafii-Tabar, H. Kamiyama, M. Cross. Molecular dynamics simulation of adsorption of Ag particles on a graphite substrate. *Surf Sci.*, **385**, 187 (1997).

[24] S.Y. Liem, K.-Y. Chan. Simulation study of platinum adsorption on graphite using the Sutton–Chen potential. *Surf Sci.*, **328**, 119 (1995).

[25] T. Cagin, Y. Kimura, Y. Qi, H. Li, H. Ikeda, W.L. Johnson, W.A. Goddard. *Bulk Metallic Glasses*, Materials Research Society, Pittsburgh (1999).